EES Catalysis

PERSPECTIVE

View Article Online
View Journal | View Issue

Cite this: *EES Catal.*, 2024, 2, 220

Reaction microenvironment control in membrane electrode assemblies for CO_2 electrolysis

Chuanchuan Yan,[ab] Dunfeng Gao, *[a] Juan-Jesús Velasco-Vélez[c] and Guoxiong Wang *[a]

Received 4th July 2023,
Accepted 13th September 2023

DOI: 10.1039/d3ey00155e

rsc.li/eescatalysis

CO_2 electrolysis is an emerging and promising carbon neutrality technology, but currently suffers from challenging selectivity issues at industrially relevant reaction rates. Selectivity control in CO_2 electrolysis relies on the molecular understanding and manipulation of multiple parallel reaction pathways that are equally governed by catalytically active sites and the reaction microenvironments in their vicinity. In this perspective, we summarize and discuss the latest achievements in reaction microenvironment control for active, selective, energy- and carbon-efficient CO_2 electrolysis, with particular attention being paid to that in membrane electrode assembly electrolyzers operating at industrial current densities ($\geq$200 mA cm^{-2}). The effects and underlying catalytic mechanisms of reaction microenvironments tailored by functional organic molecules/polymers and reactant feed compositions on the activity and selectivity of CO_2 electrolysis are discussed using selected examples. The efforts made to tailor acidic reaction microenvironments by controlling the transport of reactive species for carbon-efficient CO_2 electrolysis are also exemplified. Finally, we illustrate current challenges and future opportunities in the mechanistic understanding and rational design of reaction microenvironments for improving CO_2 electrolysis performance.

Broader context

In the context of carbon neutrality, CO_2 electrolysis has recently become a hot topic in both academia and industry, as it can electrochemically convert CO_2 to valuable chemicals and fuels under ambient conditions, with water and green electricity derived from renewable energy sources. However, CO_2 electrolysis suffers from complex reaction pathways and selectivity issues, especially at industrially relevant reaction rates. Rather than focusing on rational design of efficient catalytic materials, manipulating reaction microenvironments in the vicinity of catalytically active sites has been increasingly recognized as equally important as catalysts in tuning activity and selectivity of CO_2 electrolysis. The reaction microenvironments are closely associated with local concentrations of reactants (*e.g.*, CO_2 and H_2O) and reaction intermediates (*e.g.*, *CO, *H, and *OCCOH) as well as other reactive species (*e.g.*, H^+, OH^-, carbonate, bicarbonate, cations, and anions) at the electrode–electrolyte interface. This perspective summarizes and discusses the latest achievements in reaction microenvironment control for selective, energy- and carbon-efficient CO_2 electrolysis, with a special emphasis on that in membrane electrode assembly electrolyzers operating at industrial current densities. Strategies for effective reaction microenvironment control include molecular modification with organic molecules and polymers (ionomers), adjusting reactant feed composition, as well as tailoring acidic microenvironments.

1. Background

CO_2 electrolysis powered by renewable energy is one of the emerging technologies towards carbon neutrality. It provides a green and sustainable route that converts CO_2, water, and electricity to valuable chemicals and fuels such as CO, formate, methanol, and methane, as well as more valuable multicarbon (C_{2+}) products like ethylene, acetate, ethanol, and propanol.[1–3] As a complex electrocatalytic reaction involving carbon, hydrogen, and oxygen elements, CO_2 electrolysis suffers from many challenges in selectivity control owing to a very broad product distribution of CO_2 electroreduction, especially at industrially relevant reaction rates. The strong competition of hydrogen evolution from water electrolysis further adds complexity in controlling selectivity towards specific products. Directing CO_2 electrolysis pathways on demand is of remarkable importance for highly efficient electrocatalytic CO_2 conversion.

Since Hori's seminal works in the 1980s,[4,5] most studies on improving CO_2 electrolysis performance have been devoted to

[a] State Key Laboratory of Catalysis, Dalian National Laboratory for Clean Energy, iChEM (Collaborative Innovation Center of Chemistry for Energy Materials), Dalian Institute of Chemical Physics, Chinese Academy of Sciences, Dalian 116023, China. E-mail: dfgao@dicp.ac.cn, wanggx@dicp.ac.cn
[b] University of Chinese Academy of Sciences, Beijing 100049, China
[c] ALBA Synchrotron Light Source, Cerdanyola del Vallés, Barcelona 08290, Spain

the rational design and precise preparation of highly efficient catalytic materials.[6,7] On the other hand, similar to the surrounding environments of metal centers in enzyme catalysis, reaction microenvironments in the vicinity of catalytically active sites have been increasingly recognized as equally important as active sites for tuning activity and selectivity of heterogeneous catalytic reactions including CO_2 electrolysis.[8–11] The reaction microenvironments can modulate specific transition states and control the transport of reactive species to and from catalytically active sites, *via* multiple physicochemical effects.[9] Rationally manipulating reaction microenvironments offers an alternative strategy to break the linear scaling relationships that are widely present in heterogeneous electrocatalysis over bare metal surfaces.[12] For CO_2 electrolysis, the reaction microenvironments are closely associated with local concentrations of reactive species including reactants (*e.g.*, CO_2, H_2O), reaction intermediates (*e.g.*, *CO, *H, and *OCCOH) as well as other key species (*e.g.*, H^+, OH^-, carbonate, bicarbonate, cations, and anions) at the electrode–electrolyte interface.[13–18] Such properties are also relevant to the configurations of electrodes and electrolyzers used for CO_2 electrolysis.[19,20] A zero-gap membrane electrode assembly (MEA) electrolyzer with gas diffusion electrodes (GDEs) and solid polymer electrolytes has been recently recognized as the most advanced device towards practical application in modern electrochemistry, using which high current density and high energy efficiency can be simultaneously achieved.[21–23] In an MEA electrolyzer, liquid electrolytes or pure water and the CO_2 gas are fed to the anode and the cathode, respectively. CO_2 electrolysis proceeds at the cathode in the presence of reactive species (*e.g.*, water and cations) transported from the anode through an ion exchange membrane. Compared to the liquid–solid interfaces in traditional electrochemistry, the gas–liquid–solid three-phase electrochemical interfaces in MEA electrolyzers become much more complicated, resulting in notably distinct reaction microenvironments. In this perspective, we discuss recent advances in the reaction microenvironment control for CO_2 electrolysis, with a special emphasis on that in MEA electrolyzers operating at industrial current densities that should be $\geq$200 mA cm^{-2} in order to minimize the capital-expenditure of an electrolyzer to economically compelling levels.[24] Tailored reaction microenvironments created by organic molecules and polymers as well as reactant feed compositions for active and selective CO_2 electrolysis, as well as acidic microenvironments for carbon-efficient CO_2 electrolysis will be exemplified using selected examples (Fig. 1).

2. Tailoring reaction microenvironments by molecular modifications

In the colloidal synthesis of size- and shape-selected nanoparticle catalysts, capping agents such as small molecule

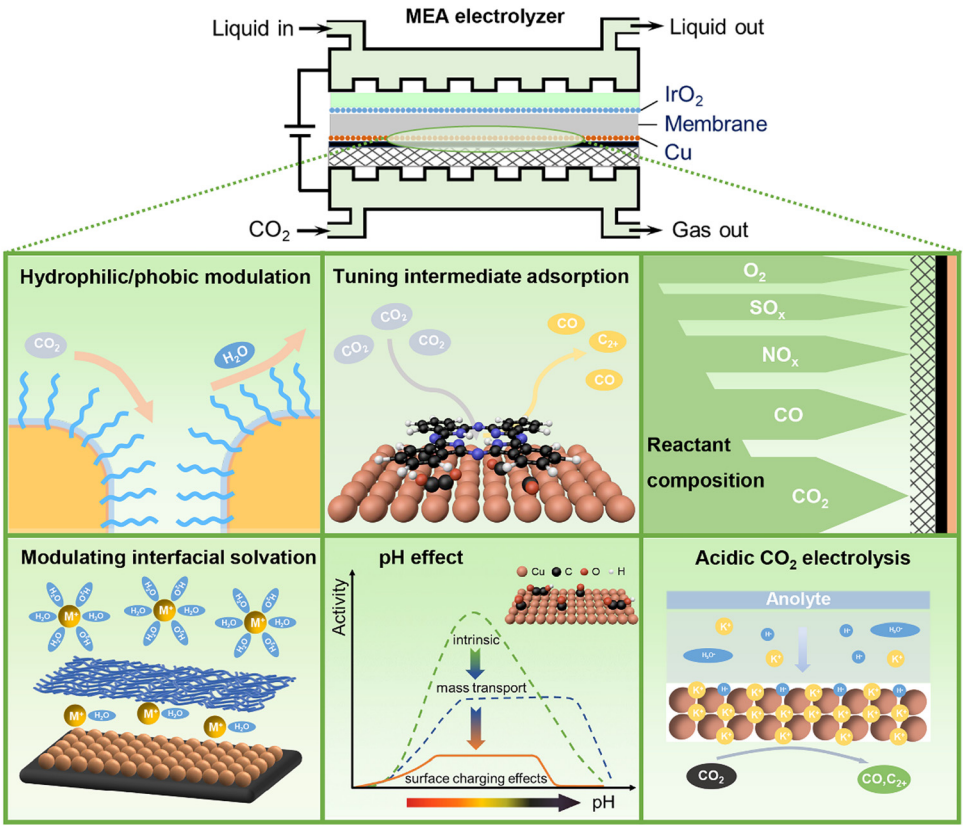

Fig. 1 Reaction microenvironment control in MEA electrolyzers for CO_2 electrolysis.

ligands and polymers are commonly used to maintain specific nanostructures by binding to metal atoms and minimizing surface energies.[25] While ligands blocking surface sites are usually considered to be detrimental to catalysis, an increasing number of reports have indicated that some ligands with appropriate design can also play a positive catalytic role in CO_2 electrolysis.[26–30] The incorporation of such ligands onto catalyst surfaces does not directly introduce alternative active sites, but would create specific reaction microenvironments that can influence the activity and selectivity of CO_2 electrolysis *via* steric and electronic effects.[26–30] These molecular modifications are expected to control reaction pathways *via* manipulating electrode hydrophilicity/hydrophobicity, modulating interfacial cation solvation, tuning the adsorption of reaction intermediates, inducing additional chemical activation of CO_2 as well as increasing ion conductivity in MEA electrolyzers.

2.1 Organic molecules and polymers

As water is a reactant for both CO_2 electrolysis and the hydrogen evolution reaction (HER), the relative local concentration of water *versus* CO_2 is a key factor affecting catalytic selectivity. Water is usually in excess, while CO_2 is insufficient under high current densities owing to limited gas diffusion from bulk liquid electrolytes or gas–liquid interfaces.[24] Organic molecules and polymers with remarkable hydrophobic character can repel water molecules surrounding catalyst surfaces and allow CO_2 gas to easily access catalyst surfaces. Mougel and co-workers developed a superhydrophobic Cu dendrite catalyst modified with 1-octadecanethiol, inspired by the gas-trapping cuticles of subaquatic spiders.[31] The hydrophobic dendritic Cu surface pushes the liquid electrolyte away to form a gas–liquid–solid triple-phase boundary at the electrode, resulting in enhanced CO_2 mass transport and thus an increased local CO_2 concentration (Fig. 2a). The bio-inspired hydrophobic electrode achieves an ethylene Faradaic efficiency (FE) of 56% and an ethanol FE of 17%, compared to 9% and 4% on an unmodified, wettable counterpart. Hydrophobic molecules are also argued to prevent interfacial water from reorientation under the action of a cathodic electric field, resulting in unfavorable water dissociation to form protons for the HER.[32] Polymers (including ionomers) are often used as binders in the preparation of catalyst layers in GDEs, and Nafion (with both hydrophilic and hydrophobic functional groups) is the most widely used binder as revealed by the knowledge from well-established fuel cell technology. Luo and co-workers further investigated two other polymer binders for Cu catalysts: polyacrylic acid (PAA, with a hydrophilic –COOH group) and fluorinated ethylene propylene (FEP, with a hydrophobic $-CF_x$ group).[33] In a flow cell, the Cu–FEP electrode exhibited a peak FE of 52% for C_{2+} products with a partial current density of over 600 mA cm^{-2}, followed by Cu–Nafion and Cu–PAA. The water contact angle follows the order of Cu–PAA < Cu–Nafion < Cu–FEP, while the captive bubble contact angle for the CO_2 bubble increases from Cu–FEP (47°) to Cu–Nafion (73°) and Cu–PAA (117°). These results suggest that electrode hydrophobicity and CO_2-philicity can be easily tuned by a thin layer of polymer binders with distinct functional groups, with the hydrophobic FEP showing the highest local CO_2/H_2O concentration ratio.

On the other hand, water is not always in excess and is likely insufficient in the case of MEA electrolyzers operating at industrial current densities when a liquid electrolyte or pure water is fed to the anode and dry CO_2 gas is fed to the cathode.

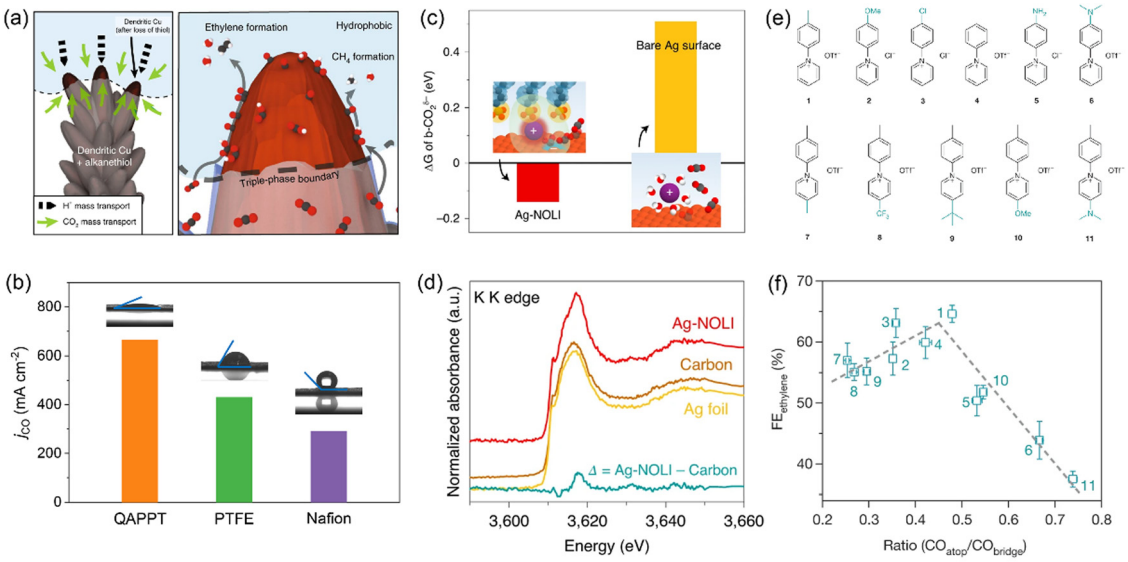

Fig. 2 (a) Illustration of the role of hydrophobicity in promoting CO_2 electroreduction over HER. Reproduced with the permission.[31] Copyright 2019, Springer Nature. (b) CO partial current densities over QAPPT-, PTFE- and Nafion-modified Ni–N–C electrodes measured in an MEA electrolyzer. Reproduced with the permission.[36] Copyright 2023, Wiley. (c) Free energy differences between physisorbed and chemisorbed CO_2 for Ag-NOLI and bare Ag surface. (d) Potassium K-edge XANES of Ag-NOLI, Ag foil, and carbon paper. Reproduced with the permission.[43] Copyright 2020, Springer Nature. (e) Molecular structures of *N*-arylpyridinium additives. (f) Correlation between ethylene FE and the ratio of $*CO_{atop}/*CO_{bridge}$ over Cu electrodes modified by dimers of *N*-arylpyridiniums in (e). Reproduced with the permission.[45] Copyright 2020, Springer Nature.

In MEA electrolyzers, water needed for CO_2 electrolysis comes from the anode through diffusion and electro-osmotic transport.[34,35] While humidified CO_2 is used in some cases, the major source of water is still the anolyte.[33,34] The excessive consumption of water at high reaction rates would significantly decrease the water concentration at the cathode, so that the low water availability limits the reaction, especially for hydrophobic catalytic materials. Using hydrophobic Ni–N–C as a model catalyst, our group investigated the role of interfacial water in CO_2 electrolysis in a custom-made alkaline MEA electrolyzer.[36] The amount of interfacial water (*i.e.*, electrode hydrophilicity/hydrophobicity) is facilely adjusted using three polymer binders: Nafion, polytetrafluoroethylene (PTFE, containing nonionic surfactants), and quaternary ammonia poly(*N*-methyl-piperidine-*co*-*p*-terphenyl) (QAPPT), as evidenced by *in situ* environmental scanning electron microscopy (ESEM) and contact angle measurements. In contrast to the Cu electrodes measured in H-cells and flow cells,[31,33,37] the hydrophilic Ni–N–C–QAPPT electrode shows the highest CO partial current density, up to 665 mA cm^{-2}, outperforming all previously reported Ni–N–C catalysts for CO_2 electrolysis (Fig. 2b). *In situ* attenuated total reflection Fourier transform infrared (ATR-FTIR) spectroscopy results indicate that increasing the amount of interfacial water modulates the mechanism of CO formation from the $*COO^-$ pathway to the *COOH pathway.[36] It is unclear whether the structure of interfacial water is also modified by different polymers, but it seems that the strategy that the HER can be suppressed by interfacial water structure modification with organic molecules or electrolyte additives in H-cells[32,38,39] does not necessarily apply to the case of MEA electrolyzers. This exceptional finding further highlights the importance of reaction microenvironment control in MEAs.

Apart from hydrophilic/phobic modulation, organic molecules and polymers can tune activity and selectivity of CO_2 electrolysis by varying local pH. Gewirth and co-workers developed a Cu–polyamine hybrid catalyst through co-electroplating and achieved an ethylene FE of 87% at −0.47 V *vs.* the reversible hydrogen electrode (RHE) in 10 M KOH electrolyte.[40] The remarkable ethylene selectivity is attributed to the higher *CO coverage and higher local pH in the presence of polyamine retained on the Cu electrode surface as revealed by the *in situ* Raman spectroscopy results. Xie and co-workers employed an anti-swelling anion exchange ionomer (AEI) to manipulate the reaction microenvironment of an oxide-derived Cu nanosheet catalyst.[41] The OH^--accumulated $-N(CH_3)_3^+$ groups and anti-swelling backbone of AEI synergistically regulated local pH and the water amount, resulting in a C_{2+} FE of 85.1% at a current density of 800 mA cm^{-2}. Bell and co-workers tailored the reaction microenvironment of a sputtered Cu catalyst using bilayer cation- and anion-conducting ionomer coatings.[10] In combination with pulsed CO_2 electrolysis, the tailored reaction microenvironment results in a 2.5-fold increase in the C_{2+} production rate with a C_{2+} FE as high as 90% compared with static electrolysis over bare Cu, owing to the higher local pH (*via* Donnan exclusion) and increased local CO_2/H_2O concentration ratio (*via* ionomer properties). Although the current densities reported in this work were low (10 to 20 mA cm^{-2}), the fundamental understanding may also be favorable for the design of membranes and ionomers for high performance MEA electrolyzers. For instance, Mallouk and co-workers introduced a weak-acid cation exchange layer *via* layer-by-layer (LBL) assembly into bipolar-membrane-based MEA electrolyzers.[42] Local pH measurements in MEA electrolyzers indicate a sharp pH increase from ∼2 to ∼5 within the first few bilayers and a steady pH in the bulk of the cation exchange layer. Thus, the presence of the weak-acid layer increased local pH near the catalyst layer and suppressed the HER current density without affecting CO_2 electroreduction.

The ligands could improve CO_2 electrolysis performance by modulating the composition, concentration, and solvation structure of interfacial cations at the electrode/electrolyte interfaces. Yang and co-workers developed a nanoparticle/ordered-ligand interlayer (NOLI) structure composed of an Ag nanoparticle surface and a detached layer of tetradecylphosphonic acid ligands in its vicinity.[43] The reversible adsorption/desorption of the ligand layer creates a catalytic pocket at the metal/ligand interface, where hydrated cations are intercalated and then lose their hydration shell due to the strong electrostatic interaction between K^+ and anionic phosphonate groups of the ligands (Fig. 2c and d). Thus, dehydrated K^+ cations are anchored close to the metal surface, stabilizing the $*COO^-$ intermediate, consistent with the cation effects correlated with hydration free energy over bare metal surfaces.[44] The modularity of NOLI is demonstrated with other anionic ligands with a long hydrocarbon chain (*e.g.*, oleic acid) and other noble metals (*e.g.*, Au, Pd). With GDE and a neutral electrolyte, the NOLI achieved a CO FE of 98.1% at 400 mA cm^{-2}.

Molecular modification provides an alternative strategy of tuning the stabilities of key intermediates to facilitate desired reaction pathways. Sargent and co-workers functionalized the surface of Cu catalysts with a library of dimers of *N*-aryl-pyridiniums (Fig. 2e) through electro-dimerization.[45] These adhered molecules improved the stabilization of the $*CO_{atop}$ intermediate (Fig. 2f), thus favoring the C–C coupling pathway *via* the dimerization of $*CO_{atop}$ and $*CO_{bridge}$. The optimal Cu catalyst modified with *N*-aryl-substituted tetrahydro-bipyridine oligomeric films achieved an impressive CO_2-to-ethylene conversion with an ethylene FE of 72% in a flow cell and a full-cell energy efficiency of 20% in an MEA electrolyzer. As *CO is a common intermediate for the formation of C_{2+} products and its coverage is relatively high compared to other intermediates (*e.g.*, *COOH, *OCCOH), many studies have been devoted to tuning the configuration and coverage of *CO adsorption by modifying Cu surfaces using ligands with versatile functional groups.[46–51] The *CO intermediate can further be enriched at the metal–organic interfaces using a tandem catalyst through functionalizing Cu surfaces with a group of porphyrin-based metallic complexes capable of reducing CO_2 to CO.[52] The interactions between ligands and complex C_2 intermediates at the molecular level would also tune relative selectivity among C_{2+} products after C–C coupling; however, relevant mechanistic understanding is still missing. Some adhered ligands could induce surface reconstruction, thus generating specific surface

sites for tuning adsorption of reaction intermediates during CO_2 electrolysis.[53–55] Whether such ligands have other direct electronic and steric effects is not yet well clarified.

The ligands may chemically activate the inert CO_2 molecule *via* specific interactions between CO_2 and functional groups such as amino, pyridyl, and imidazolium.[30] For instance, the cysteamine ligand can promote CO_2 chemisorption through hydrogen bonding with the amino group, giving rise to 53-fold enhancement in turnover frequency (TOF) for CO production over Ag.[56] By generating a highly reactive N-heterocyclic carbene (NHC) structure under reducing conditions, the imidazolium ligand can capture CO_2 to form carboxylate intermediates.[57] Wang and co-workers put forward a polyquinone modification strategy that activated CO_2 *via* quasi-reversible bonding between electrochemically reduced quinone groups and the CO_2 molecule.[58] Further incorporating the polyquinone into a Cu GDE resulted in an ethylene partial current density of 325 mA cm^{-2} at a cell voltage of 3.5 V in an MEA electrolyzer fed with pure water. In addition to CO_2 activation, the ligands may also play a physical role as a CO_2-enriching layer when dilute CO_2 is fed to GDE.[59,60]

2.2 Bifunctional ionomers

As discussed above, ionomers such as Nafion and QAPPT have been used as binders in the preparation of catalyst layers used in MEAs. However, when liquid electrolytes (*e.g.*, $KHCO_3$, KOH) are fed to MEA electrolyzers,[36,48] the ion conductivity of ionomers is not a governing factor for CO_2 electrolysis performance. In contrast, when pure water is used, the introduction of ionically conductive ionomers into catalyst layers can remarkably enlarge the electrochemical interface, as revealed by other modern polymer electrolyte-based technologies like fuel cells. CO_2 electrolysis with pure water completely avoids electrolyte consumption and corrosion issues.[21] It is highly desirable to integrate ion conductivity and chemical activation of CO_2 into one ionomer/polymer. Zhuang and co-workers developed such a bifunctional ionomer, namely, quaternary ammonia poly(ether ether ketone) (QAPEEK) with carbonyl groups in the polymer chain.[61] *In situ* ATR-SEIRAS measurements indicated that the carbonyl groups close to the electrode surface played a similar role to alkali metal cations, which helped in activating CO_2 and stabilizing the $*COO^-$ intermediate (Fig. 3a and b). The remarkable advantage of the bifunctional QAPEEK ionomer *versus* other anion exchange ionomers (*e.g.*, QAPPT, Sustainion, Fumasep, and PiperION) was verified by its drastically improved ethylene production (Fig. 3c and d). With a porous Cu catalyst, the QAPEEK ionomer helped achieving an industrial-scale ethylene partial current density of 420 mA cm^{-2} at a low cell voltage of 3.54 V without any electrolyte consumption.

3. Tailoring reaction microenvironments by reactant feed compositions

While pure CO_2 is usually used in fundamental studies of CO_2 electrolysis, the realistic composition of flue gas streams (*e.g.*, from coal-fired power plants) is very complicated. The CO_2 concentration is only 10–25% in flue gas which contains considerable amounts of N_2, unconverted O_2, trace amounts of

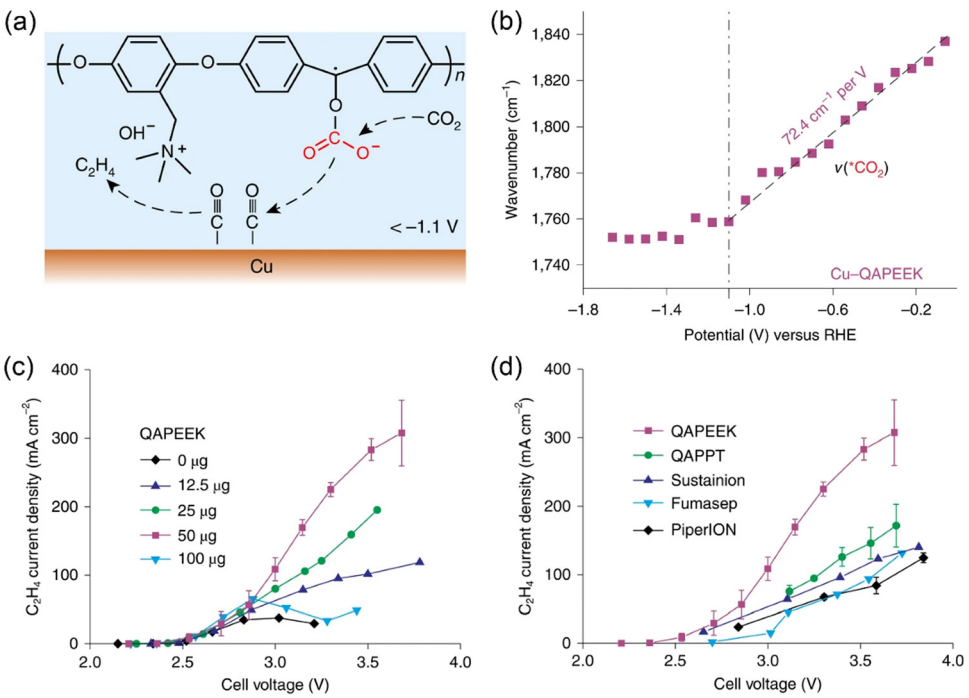

Fig. 3 (a) Schematic illustration of QAPEEK-promoted CO_2 electroreduction on Cu. (b) Potential-dependent shift of ATR-SEIRAS band of activated CO_2 ($*CO_2$) on Cu-QAPEEK. (c, d) Ethylene partial current densities of (c) Cu-QAPEEK electrodes with different amounts of QAPEEK and (d) Cu electrodes with different ionomers. Reproduced with the permission.[61] Copyright 2022, Springer Nature.

SO_x and NO_x as well as CO (due to incomplete combustion). Direct electrolysis of CO_2 from such industrial sources is necessary but very challenging. On the other hand, the presence of these impurities in the feed would also change the reaction microenvironments for CO_2 electrolysis.

The reduction of O_2 is thermodynamically favorable over that of CO_2; so it is urgently needed to develop O_2-tolerant electrodes. A polymer of intrinsic microporosity[62] and a hydrated ionomer catalyst coating[63] have been developed to locally slow O_2 transport as a CO_2-selective layer on the electrodes. The presence of O_2 in the feed is also argued to facilitate CO_2 electrolysis by stabilizing surface Cu oxide or oxyhydroxide species.[64,65] The presence of a trace amount of NO_x shows a negligible impact on CO_2 electrolysis despite loss in FE due to the facile electroreduction of NO_x,[65,66] while SO_x could poison Cu catalysts and suppress the C_{2+} production.[65,67] Another important feature of flue gas is its low CO_2 concentration which limits CO_2 electrolysis rate owing to the first-order reaction kinetics. This issue stimulates a new research direction, namely, integrated CO_2 capture and electroreduction technologies.[59,68,69] Coating a layer of organic ligands onto catalyst surfaces to enrich CO_2 and increase the local CO_2 concentration in reaction microenvironments is an effective method to improve electrolysis performance of dilute CO_2 feed.[59]

The flue gas from steel plants contains a large fraction of CO, and simultaneous conversion of CO_2 and CO is desirable. The co-electrolysis of CO_2/CO is rarely studied to date, and the underlying co-electrolysis mechanism is also under debate. The promoting effect of cross-coupling of CO_2/CO and the major contribution from CO_2 or CO alone have been proposed.[70–74] These studies are conducted in H-cells with neutral electrolytes. Our group conducted CO_2/CO co-electrolysis in an alkaline MEA electrolyzer where reaction microenvironments were quite different from those in H-cells.[65] An obvious difference was the available CO_2/CO concentration which was close to that in the CO_2/CO feeds in MEAs without being affected by CO_2/CO solubility. With increasing CO pressure in the feed, the major product gradually shifted from ethylene to acetate and meanwhile the current density increased drastically (Fig. 4a). Under optimized reaction conditions, C_{2+} FE and partial current density reached 90.0% and 3.1 A cm^{-2}, respectively. Structural characterization, control experiments with Ar/CO co-feeds, isotopic labeling experiments, and *operando* Raman spectroscopy measurements (Fig. 4b–e) indicated that the feed-composition-dependent selectivity changes were not ascribed to any structural changes, but were induced by reaction microenvironments, herein, *CO coverage (by the pressure of CO) and local pH (by the ratio of CO_2). It should be noted that CO_2–CO cross-coupling did occur in CO_2/CO co-electrolysis under MEA conditions,[65] but did not improve the formation of ethylene.[70,74] The insights presented in our work highlight the great importance of both reactant feed composition and electrolyzer configuration in the reaction microenvironment control for selective production of single products.

4. Tailoring reaction microenvironments in acidic CO_2 electrolysis

A challenging issue of CO_2 electrolysis in alkaline and neutral media is carbonate formation and crossover which leads to

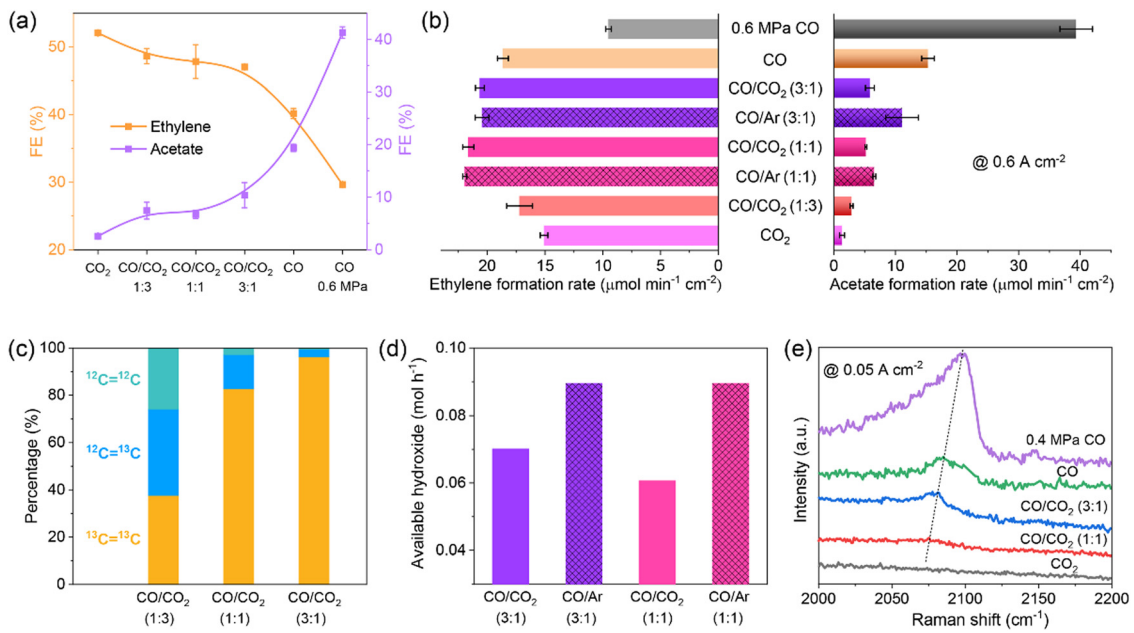

Fig. 4 (a) FEs and (b) formation rates of ethylene and acetate, (c) molar ratios of $^{12}CH_2{=}{=}^{12}CH_2$, $^{12}CH_2{=}{=}^{13}CH_2$, and $^{13}CH_2{=}{=}^{13}CH_2$ in produced ethylene, (d) available OH^- formation rates, and (e) *operando* $*CO_{atop}$ Raman peaks over CuO nanosheet catalyst measured with different feeds. Reproduced with the permission.[65] Copyright 2023, Springer Nature.

substantial CO_2 loss, high cost for downstream CO_2 regeneration and separation, as well as reduced long-term electrolyzer stability.[75] Strategies such as rinsing GDEs with water, applying periodic regeneration voltage and using bipolar membranes (BPMs) have been proposed to alleviate the effects of carbonate formation,[76–78] but failed to address this issue by eliminating its formation intrinsically. The origin of the carbonate formation is the homogeneous reaction of CO_2 with OH^- that is present in electrolytes or is formed as a side product of proton consumption *via* the reduction of CO_2 and water. The latter would be the major OH^- source for the carbonate formation in MEA electrolyzers operating at industrial current densities. CO_2 crossover occurs *via* electromigration of carbonate or bicarbonate ions from the cathode to anode through an anion exchange membrane. The Bjerrum plot of the carbonate system suggests that the formation of carbonate and bicarbonate can be completely suppressed at a pH lower than 4. Therefore, CO_2 electrolysis in acidic media holds great promise in achieving carbon-efficient CO_2 conversion. Given the remarkable interfacial pH increase upon applying high current densities as revealed by the reaction–diffusion modelling results,[79] reaction media should be strongly acidic, ideally with a bulk pH lower than 2, in order to fully eliminate the carbonate formation. However, such harsh reaction conditions give rise to extra difficulty in selectivity control owing to facile HER and unfavorable C–C coupling.

Many attempts have been made to improve acidic CO_2 electrolysis by tailoring reaction microenvironments, for instance, creating a locally alkaline environment and increasing the cation concentration near catalyst surfaces.[80–83] Sinton and co-workers developed a cation-carrying and proton-blocking catalyst adlayer to suppress HER and promote CO_2 electrolysis to C_{2+} products.[84] The adlayer was composed of insulating polymer nanoparticles (IPN, imine- and carbonyl-functionalized covalent organic frameworks) and perfluorinated sulfonic-acid (PFSA) ionomers, and it can restrict proton transport flux to cation-conducting hydrophilic nanochannels and enrich K^+ near the Cu catalyst surface (Fig. 5a). The resulting high local alkalinity and cation-enriched reaction microenvironment enabled a C_{2+} FE of 75% and a single-pass CO_2 utilization of 45% towards C_{2+} at 200 mA cm^{-2} in a slim flow cell. The asymmetric ion migration–adsorption strategy has also been verified *via* modifying catalyst surfaces with covalent organic frameworks and organic additives.[85,86] In addition to manipulating local cation concentrations, such molecular modifications were also expected to exhibit other direct microenvironment effects by interacting with intermediates, similar to the case of alkaline electrolysis discussed above (Section 2). Our group developed an acidic MEA electrolyzer using K_2SO_4 + H_2SO_4 anolytes with pH 0–2 and used HER-inactive Ni–N–C as a model catalyst.[87] By optimizing pH, K^+ concentration and CO_2 pressure, acidic CO_2 electrolysis achieved a CO FE of 95% at a total current density of 500 mA cm^{-2} at pH 0.5 and the CO_2 loss can be reduced by 86% at 300 mA cm^{-2}, compared with alkaline CO_2 electrolysis (Fig. 5b–d). By further adjusting the flow rate of input CO_2, the single-pass CO_2 utilization reached

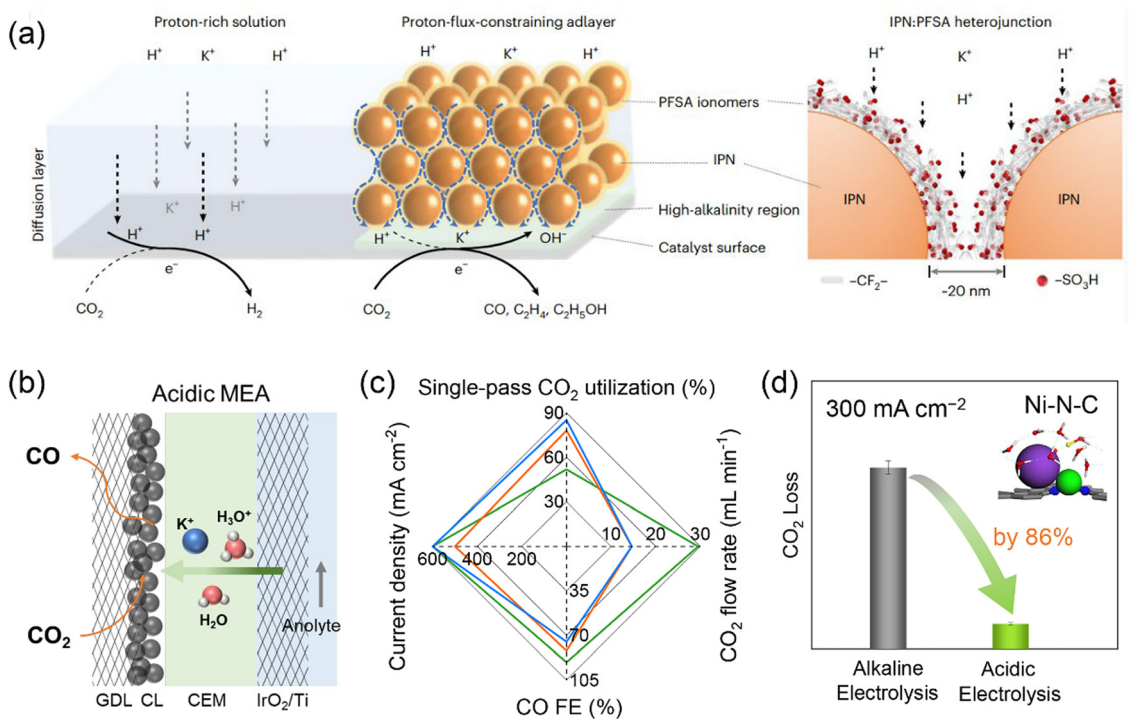

Fig. 5 (a) Reaction microenvironment control in strong acid *via* proton-flux-constraining ionomer adlayer design. Reproduced with the permission.[84] Copyright 2023, Springer Nature. (b) Schematic representation of acidic MEA electrolyzer. (c) Acidic CO_2 electrolysis performance over Ni–N–C catalyst. (d) Comparison of CO_2 loss in acidic electrolysis (0.5 M K_2SO_4 + H_2SO_4 anolyte with pH 0.5, 0.5 MPa CO_2) and alkaline electrolysis (1 M KOH anolyte, 0.5 MPa CO_2) over Ni–N–C catalyst. Reproduced with the permission.[87] Copyright 2023, Royal Society of Chemistry.

as high as 85%, breaking the upper limit of 50% for CO production in alkaline CO_2 electrolysis. The impressive CO selectivity at high current densities was attributed to the presence of high-concentration K^+ cations that migrated from the anolyte. Li and co-workers also achieved a CO FE of ~80% and a single-pass CO_2 utilization of ~90% in an acidic MEA electrolyzer using Cs^+ cations and Ag catalyst.[88] It seemed that high-concentration cations were indispensable for efficient acidic CO_2 electrolysis. A couple of mechanisms on cation effects have been proposed, such as interfacial electric field, buffering interfacial pH, stabilizing intermediates and non-electric field effect.[18] All the proposed reaction mechanisms were positively correlated with cation concentration. Further investigations on producing C_{2+} products in acidic MEA electrolyzers are still needed, due to relatively facile HER performance of Cu catalysts and the limited local cation concentration in MEA configurations. It should be noted that for acidic CO_2 electrolysis in anolyte-fed MEA electrolyzers, salt deposition still occurred at an extended electrolysis period, especially when using high-concentration cations due to the transfer of cations from the anolyte to cathode through membranes.[87] Replacing alkali metal cations with organic cations or cationic functional groups/ionomers likely achieved sustainable CO_2 electrolysis under acidic conditions or even with pure water.[61,89–91] This strategy has recently shown great promise, but whether the catalytic capability of these organic cations is comparable to that of alkali metal cations is still not yet clear. Given that CO does not react with OH^- to form carbonate and C_{2+} selectivity of CO electrolysis is higher, tandem acidic/alkaline electrolysis, namely, connecting an acidic MEA electrolyzer (CO_2 electrolysis to CO) and an alkaline MEA electrolyzer (CO electrolysis to C_{2+}), has been proposed and demonstrated as an energy- and carbon-efficient route for CO_2 electrolysis to C_{2+} products.[87]

5. Conclusions and outlook

In this perspective, we have summarized and discussed the fundamentals and strategies of tuning reaction microenvironments for active, selective, energy- and carbon-efficient CO_2 electrolysis, with particular attention being paid to those examples using MEA electrolyzers towards practical applications. The effects and underlying mechanisms of reaction microenvironments created by molecular modifications with organic molecules/polymers and tuned by reactant feed compositions on the activity and selectivity of CO_2 electrolysis are illustrated in detail. The efforts to rationally control the transport of H^+/OH^- and cations to modify acidic reaction microenvironments for carbon-efficient CO_2 electrolysis are also discussed. The presented examples and associated mechanistic insights highlight future opportunities and design strategies towards reaction microenvironment control for improved activity and selectivity of CO_2 electrolysis.

Despite the recent achievements, the intrinsic underlying effects of reaction microenvironments around catalytically active sites are not understood in depth. For instance, molecular modification of catalyst surfaces is the most widely studied case of reaction microenvironment control, but multiple likely effects (*e.g.*, due to hydrophobicity, local pH, intermediate stabilization, and ion transport) often co-exist in one catalyst system and are difficult to be decoupled. Although control experiments can be performed to rule out contributions of some factors, it is hardly realistic to precisely control ligand structures, catalyst surface structures as well as their complicated interactions, especially under industrially relevant harsh conditions. Currently, the enhancement in C_{2+} production has been demonstrated with the aid of tailored reaction microenvironments of Cu catalysts and has been mainly ascribed to the enrichment and activation of CO_2 and the improved adsorption of key intermediates such as *CO.[10,36,43,45,61] However, how the organic ligands interact with more complex intermediates beyond $*CO_2$ and *CO at the molecular level is still not yet clarified. The precise molecular control over specific interactions between ligands and intermediates would be favorable for tuning selectivity among C_{2+} products and generating specific C_{2+} products.[92] Advanced *operando* spectroscopy and microscopy characterization with sufficient temporal and spatial resolution would help in resolving the exact structures of catalysts and ligands in these systems.[42,93–97]

In addition to initial states and conditions, reaction microenvironments are also dynamic and closely associated with reaction rates. As the mass transport of reactive species (*e.g.*, CO_2, H_2O, H^+, OH^-, carbonate, bicarbonate, cations, and intermediates) at the mesoscale in the reaction microenvironments significantly influences reaction kinetics, their concentration profiles at the electrode/electrolyte interface should be accurately determined *via* experimental measurements under reaction conditions and/or multiphysics simulations using reasonable reaction–diffusion models.[35,79,98–102] The reaction microenvironments in MEAs (*e.g.*, membrane, ionomer, and catalyst layer structure) are more complex, but currently not well-investigated yet, adding extra degrees of freedom for activity and selectivity control, especially in acidic CO_2 electrolysis. We believe that revealing the nature of electrocatalytic interfaces at the mesoscale would help in designing customizable reaction microenvironments for active, selective, energy- and carbon-efficient CO_2 electrolysis.

Conflicts of interest

There are no conflicts to declare.

Acknowledgements

This work was supported by the National Key R&D Program of China (2022YFA1504603), the National Natural Science Foundation of China (22002155, 22372171, 22125205, and 92045302), the Fundamental Research Funds for the Central Universities (20720220008), the Natural Science Foundation of Liaoning Province (2021-MS-022), the Liao Ning Revitalization

Talents Program, the Dalian Institute of Chemical Physics (DICP I202203) and the Photon Science Center for Carbon Neutrality.

References

1 P. De Luna, C. Hahn, D. Higgins, S. A. Jaffer, T. F. Jaramillo and E. H. Sargent, *Science*, 2019, **364**, eaav3506.
2 I. E. L. Stephens, K. Chan, A. Bagger, S. W. Boettcher, J. Bonin, E. Boutin, A. K. Buckley, R. Buonsanti, E. R. Cave, X. X. Chang, S. W. Chee, A. H. M. da Silva, P. de Luna, O. Einsle, B. Endrodi, M. Escudero-Escribano, J. V. F. de Araujo, M. C. Figueiredo, C. Hahn, K. U. Hansen, S. Haussener, S. Hunegnaw, Z. Y. Huo, Y. J. Hwang, C. Janaky, B. S. Jayathilake, F. Jiao, Z. P. Jovanov, P. Karimi, M. T. M. Koper, K. P. Kuhl, W. H. Lee, Z. Q. Liang, X. Liu, S. C. Ma, M. Ma, H. S. Oh, M. Robert, B. Roldan Cuenya, J. Rossmeisl, C. Roy, M. P. Ryan, E. H. Sargent, P. Sebastian-Pascual, B. Seger, L. Steier, P. Strasser, A. S. Varela, R. E. Vos, X. Wang, B. J. Xu, H. Yadegari and Y. X. Zhou, *J. Phys. Energy*, 2022, **4**, 042003.
3 D. F. Gao, W. J. Li, H. Y. Wang, G. X. Wang and R. Cai, *Trans. Tianjin Univ.*, 2022, **28**, 245–264.
4 Y. Hori, K. Kikuchi and S. Suzuki, *Chem. Lett.*, 1985, 1695–1698.
5 Y. Hori, K. Kikuchi, A. Murata and S. Suzuki, *Chem. Lett.*, 1986, 897–898.
6 Y. Y. Birdja, E. Perez-Gallent, M. C. Figueiredo, A. J. Gottle, F. Calle-Vallejo and M. T. M. Koper, *Nat. Energy*, 2019, **4**, 732–745.
7 D. F. Gao, R. M. Aran-Ais, H. S. Jeon and B. Roldan Cuenya, *Nat. Catal.*, 2019, **2**, 198–210.
8 H. B. Li, J. P. Xiao, Q. Fu and X. H. Bao, *Proc. Natl. Acad. Sci. U. S. A.*, 2017, **114**, 5930–5934.
9 A. R. Riscoe, C. J. Wrasman, A. A. Herzing, A. S. Hoffman, A. Menon, A. Boubnov, M. Vargas, S. R. Bare and M. Cargnello, *Nat. Catal.*, 2019, **2**, 852–863.
10 C. Kim, J. C. Bui, X. Y. Luo, J. K. Cooper, A. Kusoglu, A. Z. Weber and A. T. Bell, *Nat. Energy*, 2021, **6**, 1026–1034.
11 J. X. Guo, Y. Zheng, Z. P. Hu, C. Y. Zheng, J. Mao, K. Du, M. Jaroniec, S. Z. Qiao and T. Ling, *Nat. Energy*, 2023, **8**, 264–272.
12 Y. Lai, N. B. Watkins, A. Rosas-Hernandez, A. Thevenon, G. P. Heim, L. Zhou, Y. S. Wu, J. C. Peters, J. M. Gregoire and T. Agapie, *ACS Cent. Sci.*, 2021, **7**, 1756–1762.
13 Y. J. Sa, C. W. Lee, S. Y. Lee, J. Na, U. Lee and Y. J. Hwang, *Chem. Soc. Rev.*, 2020, **49**, 6632–6665.
14 J. C. Bui, C. Kim, A. J. King, O. Romiluyi, A. Kusoglu, A. Z. Weber and A. T. Bell, *Acc. Chem. Res.*, 2022, **55**, 484–494.
15 A. N. Xu, N. Govindarajan, G. Kastlunger, S. Vijay and K. R. Chan, *Acc. Chem. Res.*, 2022, **55**, 495–503.
16 B. W. Deng, M. Huang, X. L. Zhao, S. Y. Mou and F. Dong, *ACS Catal.*, 2022, **12**, 331–362.
17 J. J. Lv, R. N. Yin, L. M. Zhou, J. Li, R. Kikas, T. Xu, Z. J. Wang, H. L. Jin, X. Wang and S. Wang, *Angew. Chem., Int. Ed.*, 2022, **61**, e202207252.
18 Y. W. Rong, J. Q. Sang, L. Che, D. F. Gao and G. X. Wang, *Acta Phys.-Chim. Sin.*, 2023, **39**, 2212027.
19 D. Wakerley, S. Lamaison, J. Wicks, A. Clemens, J. Feaster, D. Corral, S. A. Jaffer, A. Sarkar, M. Fontecave, E. B. Duoss, S. Baker, E. H. Sargent, T. F. Jaramillo and C. Hahn, *Nat. Energy*, 2022, **7**, 130–143.
20 D. F. Gao, P. F. Wei, H. F. Li, L. Lin, G. X. Wang and X. H. Bao, *Acta Phys.-Chim. Sin.*, 2021, **37**, 2009021.
21 Z. L. Yin, H. Q. Peng, X. Wei, H. Zhou, J. Gong, M. M. Huai, L. Xiao, G. W. Wang, J. T. Lu and L. Zhuang, *Energy Environ. Sci.*, 2019, **12**, 2455–2462.
22 L. Ge, H. Rabiee, M. R. Li, S. Subramanian, Y. Zheng, J. H. Lee, T. Burdyny and H. Wang, *Chem*, 2022, **8**, 663–692.
23 Z. Zhang, X. Huang, Z. Chen, J. J. Zhu, B. Endrodi, C. Janaky and D. H. Deng, *Angew. Chem., Int. Ed.*, 2023, **62**, e202302789.
24 T. Burdyny and W. A. Smith, *Energy Environ. Sci.*, 2019, **12**, 1442–1453.
25 K. An and G. A. Somorjai, *ChemCatChem*, 2012, **4**, 1512–1524.
26 J. G. Wang, F. Q. Zhang, X. W. Kang and S. W. Chen, *Curr. Opin. Electrochem.*, 2019, **13**, 40–46.
27 A. Wagner, C. D. Sahm and E. Reisner, *Nat. Catal.*, 2020, **3**, 775–786.
28 D. H. Nam, P. De Luna, A. Rosas-Hernandez, A. Thevenon, F. W. Li, T. Agapie, J. C. Peters, O. Shekhah, M. Eddaoudi and E. H. Sargent, *Nat. Mater.*, 2020, **19**, 266–276.
29 M. Jun, D. Kim, M. Kim, M. Kim, T. Kwon and K. Lee, *ACS Omega*, 2022, **7**, 42655–42663.
30 Q. S. Zhu, C. J. Murphy and L. R. Baker, *J. Am. Chem. Soc.*, 2022, **144**, 2829–2840.
31 D. Wakerley, S. Lamaison, F. Ozanam, N. Menguy, D. Mercier, P. Marcus, M. Fontecave and V. Mougel, *Nat. Mater.*, 2019, **18**, 1222–1227.
32 S. J. Mu, L. Li, R. J. Zhao, H. L. Lu, H. L. Dong and C. H. Cui, *ACS Appl. Mater. Interfaces*, 2021, **13**, 47619–47628.
33 T. H. Pham, J. Zhang, M. Li, T. H. Shen, Y. Ko, V. Tileli, W. Luo and A. Zuttel, *Adv. Energy Mater.*, 2022, **12**, 2103663.
34 W. Choi, S. Park, W. Jung, D. H. Won, J. Na and Y. J. Hwang, *ACS Energy Lett.*, 2022, **7**, 939–945.
35 W. Choi, Y. Choi, E. Choi, H. Yun, W. Jung, W. H. Lee, H. S. Oh, D. H. Won, J. Na and Y. J. Hwang, *J. Mater. Chem. A*, 2022, **10**, 10363–10372.
36 P. F. Wei, H. F. Li, R. T. Li, Y. Wang, T. F. Liu, R. Cai, D. F. Gao, G. X. Wang and X. H. Bao, *Small*, 2023, **19**, 202300856.
37 A. Kormányos, B. Endrődi, Z. Zhang, A. Samu, L. Mérai, G. F. Samu, L. Janováka and C. Janáky, *EES Catal.*, 2023, **1**, 263–273.
38 Z. Q. Zhang, S. Banerjee, V. S. Thoi and A. S. Hall, *J. Phys. Chem. Lett.*, 2020, **11**, 5457–5463.
39 N. Mohandas, T. N. Narayanan and A. Cuesta, *ACS Catal.*, 2023, **13**, 8384–8393.
40 X. Y. Chen, J. F. Chen, N. M. Alghoraibi, D. A. Henckel, R. X. Zhang, U. O. Nwabara, K. E. Madsen, P. J. A. Kenis, S. C. Zimmerman and A. A. Gewirth, *Nat. Catal.*, 2021, **4**, 20–27.

41 Y. Zhao, X. L. Zu, R. H. Chen, X. D. Li, Y. W. Jiang, Z. Q. Wang, S. M. Wang, Y. Wu, Y. F. Sun and Y. Xie, *J. Am. Chem. Soc.*, 2022, **144**, 10446–10454.
42 Z. F. Yan, J. L. Hitt, Z. C. Zeng, M. A. Hickner and T. E. Mallouk, *Nat. Chem.*, 2021, **13**, 33–40.
43 D. Kim, S. Yu, F. Zheng, I. Roh, Y. F. Li, S. Louisia, Z. Y. Qi, G. A. Somorjai, H. Frei, L. W. Wang and P. D. Yang, *Nat. Energy*, 2020, **5**, 1032–1042.
44 V. J. Ovalle, Y. S. Hsu, N. Agrawal, M. J. Janik and M. M. Waegele, *Nat. Catal.*, 2022, **5**, 624–632.
45 F. W. Li, A. Thevenon, A. Rosas-Hernández, Z. Y. Wang, Y. L. Li, C. M. Gabardo, A. Ozden, C. T. Dinh, J. Li, Y. H. Wang, J. P. Edwards, Y. Xu, C. McCallum, L. Z. Tao, Z. Q. Liang, M. C. Luo, X. Wang, H. H. Li, C. P. O'Brien, C. S. Tan, D. H. Nam, R. Quintero-Bermudez, T. T. Zhuang, Y. G. C. Li, Z. J. Han, R. D. Britt, D. Sinton, T. Agapie, J. C. Peters and E. H. Sargent, *Nature*, 2020, **577**, 509–513.
46 Y. Shi, K. Sun, J. Shan, H. Li, J. Gao, Z. Chen, C. Sun, Y. Shuai and Z. Wang, *ACS Catal.*, 2022, **12**, 8252–8258.
47 P. Ding, H. Y. An, P. Zellner, T. F. Guan, J. Y. Gao, P. Muller-Buschbaum, B. M. Weckhuysen, W. van der Stam and I. D. Sharp, *ACS Catal.*, 2023, **13**, 5336–5347.
48 A. Ozden, F. W. Li, F. P. G. de Arquer, A. Rosas-Hernandez, A. Thevenon, Y. H. Wang, S. F. Hung, X. Wang, B. Chen, J. Li, J. Wicks, M. C. Luo, Z. Y. Wang, T. Agapie, J. C. Peters, E. H. Sargent and D. Sinton, *ACS Energy Lett.*, 2020, **5**, 2811–2818.
49 M. S. Xie, B. Y. Xia, Y. W. Li, Y. Yan, Y. H. Yang, Q. Sun, S. H. Chan, A. Fisher and X. Wang, *Energy Environ. Sci.*, 2016, **9**, 1687–1695.
50 L. Fan, C. Y. Liu, P. Zhu, C. Xia, X. Zhang, Z. Y. Wu, Y. Y. Lu, T. P. Senftle and H. T. Wang, *Joule*, 2022, **6**, 205–220.
51 Q. Chang, J. H. Lee, Y. Liu, Z. Xie, S. Hwang, N. S. Marinkovic, A. H. A. Park, S. Kattel and J. G. Chen, *JACS Au*, 2022, **2**, 214–222.
52 F. W. Li, Y. G. C. Li, Z. Y. Wang, J. Li, D. H. Nam, Y. Lum, M. C. Luo, X. Wang, A. Ozden, S. F. Hung, B. Chen, Y. H. Wang, J. Wicks, Y. Xu, Y. L. Li, C. M. Gabardo, C. T. Dinh, Y. Wang, T. T. Zhuang, D. Sinton and E. H. Sargent, *Nat. Catal.*, 2020, **3**, 75–82.
53 H. L. Wu, J. Li, K. Qi, Y. Zhang, E. Petit, W. S. Wang, V. Flaud, N. Onofrio, B. Rebiere, L. Q. Huang, C. Salameh, L. Lajaunie, P. Miele and D. Voiry, *Nat. Commun.*, 2021, **12**, 7210.
54 X. R. He, J. W. Chen, Y. F. Xu, Y. Shen, Y. F. Zeng, J. Y. Zhu, B. J. Xu and C. Wang, *Nano Res.*, 2023, **16**, 4554–4561.
55 C. F. Cheng, T. F. Liu, Y. Wang, P. F. Wei, J. Q. Sang, J. Q. Shao, Y. P. Song, Y. P. Zang, D. F. Gao and G. X. Wang, *J. Energy Chem.*, 2023, **81**, 125–131.
56 Z. J. Wang, L. N. Wu, K. Sun, T. Chen, Z. H. Jiang, T. Cheng and W. A. Goddard, *J. Phys. Chem. Lett.*, 2018, **9**, 3057–3061.
57 J. Tamura, A. Ono, Y. Sugano, C. C. Huang, H. Nishizawa and S. Mikoshiba, *Phys. Chem. Chem. Phys.*, 2015, **17**, 26072–26078.
58 J. M. Li, F. F. Li, C. Liu, F. Y. Wei, J. Gong, W. Z. Li, L. W. Xue, J. L. Yin, L. Xiao, G. W. Wang, J. T. Lu and L. Zhuang, *ACS Energy Lett.*, 2022, **7**, 4045–4051.
59 Y. Y. Cheng, J. Hou and P. Kang, *ACS Energy Lett.*, 2021, **6**, 3352–3358.
60 J. C. Wang, T. Cheng, A. Q. Fenwick, T. N. Baroud, A. Rosas-Hernandez, J. H. Ko, Q. Gan, W. A. Goddard and R. H. Grubbs, *J. Am. Chem. Soc.*, 2021, **143**, 2857–2865.
61 W. Z. Li, Z. L. Yin, Z. Y. Gao, G. W. Wang, Z. Li, F. Y. Wei, X. Wei, H. Q. Peng, X. T. Hu, L. Xiao, J. T. Lu and L. Zhuang, *Nat. Energy*, 2022, **7**, 835–843.
62 X. Lu, Z. Jiang, X. L. Yuan, Y. S. Wu, R. Malpass-Evans, Y. R. Zhong, Y. Y. Liang, N. B. McKeown and H. L. Wang, *Sci. Bull.*, 2019, **64**, 1890–1895.
63 Y. Xu, J. P. Edwards, J. J. Zhong, C. P. O'Brien, C. M. Gabardo, C. McCallum, J. Li, C. T. Dinh, E. H. Sargent and D. Sinton, *Energy Environ. Sci.*, 2020, **13**, 554–561.
64 M. He, C. S. Li, H. C. Zhang, X. X. Chang, J. G. G. Chen, W. A. Goddard, M. J. Cheng, B. J. Xu and Q. Lu, *Nat. Commun.*, 2020, **11**, 3844.
65 P. F. Wei, D. F. Gao, T. F. Liu, H. F. Li, J. Q. Sang, C. Wang, R. Cai, G. X. Wang and X. H. Bao, *Nat. Nanotechnol.*, 2023, **18**, 299–306.
66 B. H. Ko, B. Hasa, H. Shin, E. Jeng, S. Overa, W. Chen and F. Jiao, *Nat. Commun.*, 2020, **11**, 5856.
67 W. Luc, B. H. Ko, S. Kattel, S. Li, D. Su, J. G. G. Chen and F. Jiao, *J. Am. Chem. Soc.*, 2019, **141**, 9902–9909.
68 A. Prajapati, R. Sartape, M. T. Galante, J. H. Xie, S. L. Leung, I. Bessa, M. H. S. Andrade, R. T. Somich, M. V. Reboucas, G. T. Hutras, N. Diniz and M. R. Singh, *Energy Environ. Sci.*, 2022, **15**, 5105–5117.
69 G. Lee, A. S. Rasouli, B. Lee, J. Zhang, D. H. Won, Y. C. Xiao, J. P. Edwards, M. G. Lee, E. D. Jung, F. Arabyarmohammadi, H. Liu, I. Grigioni, J. Abed, T. Alkayyali, S. Liu, K. Xie, R. K. Miao, S. Park, R. Dorakhan, Y. Zhao, C. P. O'Brien, Z. Chen, D. Sinton and E. H. Sargent, *Joule*, 2023, **7**, 1277–1288.
70 X. L. Wang, J. F. de Araujo, W. Ju, A. Bagger, H. Schmies, S. Kuhl, J. Rossmeisl and P. Strasser, *Nat. Nanotechnol.*, 2019, **14**, 1063–1070.
71 N. S. R. Cuellar, C. Scherer, B. Kackar, W. Eisenreich, C. Huber, K. Wiesner-Fleischer, M. Fleischer and O. Hinrichsen, *J. CO_2* Util., 2020, **36**, 263–275.
72 M. Moradzaman and G. Mul, *J. Phys. Chem. C*, 2021, **125**, 6546–6554.
73 J. Gao, A. Bahmanpour, O. Krocher, S. M. Zakeeruddin, D. Ren and M. Gratzel, *Nat. Chem.*, 2023, **15**, 705–713.
74 W. Gao, Y. Xu, L. Fu, X. Chang and B. Xu, *Nat. Catal.*, 2023, DOI: **10.1038/s41929-023-01002-6**.
75 M. Sassenburg, M. Kelly, S. Subramanian, W. A. Smith and T. Burdyny, *ACS Energy Lett.*, 2023, **8**, 321–331.
76 B. De Mot, M. Ramdin, J. Hereijgers, T. J. H. Vlugt and T. Breugelmans, *ChemElectroChem*, 2020, **7**, 3839–3843.
77 Y. Xu, J. P. Edwards, S. J. Liu, R. K. Miao, J. E. Huang, C. M. Gabardo, C. P. O'Brien, J. Li, E. H. Sargent and D. Sinton, *ACS Energy Lett.*, 2021, **6**, 809–815.
78 K. Xie, R. K. Miao, A. Ozden, S. J. Liu, Z. Chen, C. T. Dinh, J. E. Huang, Q. C. Xu, C. M. Gabardo, G. Lee, J. P. Edwards,

C. P. O'Brien, S. W. Boettcher, D. Sinton and E. H. Sargent, *Nat. Commun.*, 2022, **13**, 3609.
79 Y. Xie, P. F. Ou, X. Wang, Z. Y. Xu, Y. C. Li, Z. Y. Wang, J. E. Huang, J. Wicks, C. McCallum, N. Wang, Y. H. Wang, T. X. Chen, B. T. W. Lo, D. Sinton, J. C. Yu, Y. Wang and E. H. Sargent, *Nat. Catal.*, 2022, **5**, 564–570.
80 C. P. O'Brien, R. K. Miao, S. J. Liu, Y. Xu, G. Lee, A. Robb, J. E. Huang, K. Xie, K. Bertens, C. M. Gabardo, J. P. Edwards, C. T. Dinh, E. H. Sargent and D. Sinton, *ACS Energy Lett.*, 2021, **6**, 2952–2959.
81 Z. S. Ma, Z. L. Yang, W. C. Lai, Q. Y. Wang, Y. Qiao, H. L. Tao, C. Lian, M. Liu, C. Ma, A. L. Pan and H. W. Huang, *Nat. Commun.*, 2022, **13**, 7596.
82 X. D. Sheng, W. X. Ge, H. L. Jiang and C. Z. Li, *Adv. Mater.*, 2022, **34**, e202201295.
83 Z. Jiang, Z. S. Zhang, H. Li, Y. R. Tang, Y. B. Yuan, J. Zao, H. Z. Zheng and Y. Y. Liang, *Adv. Energy Mater.*, 2023, **13**, e202203603.
84 Y. Zhao, L. Hao, A. Ozden, S. Liu, R. K. Miao, P. Ou, T. Alkayyali, S. Zhang, J. Ning, Y. Liang, Y. Xu, M. Fan, Y. Chen, J. E. Huang, K. Xie, J. Zhang, C. P. O'Brien, F. Li, E. H. Sargent and D. Sinton, *Nat. Synth.*, 2023, **2**, 403–412.
85 A. Ozden, J. Li, S. Kandambeth, X. Y. Li, S. J. Liu, O. Shekhah, P. F. Ou, Y. Z. Finfrock, Y. K. Wang, T. Alkayyali, F. P. G. de Arquer, V. S. Kale, P. M. Bhatt, A. H. Ip, M. Eddaoudi, E. H. Sargent and D. Sinton, *Nat. Energy*, 2023, **8**, 179–190.
86 W. X. Nie, G. P. Heim, N. B. Watkins, T. Agapie and J. C. Peters, *Angew. Chem. Int. Ed.*, 2023, **62**, e202216102.
87 H. F. Li, H. B. Li, P. F. Wei, Y. Wang, Y. P. Zang, D. F. Gao, G. X. Wang and X. H. Bao, *Energy Environ. Sci.*, 2023, **16**, 1502–1510.
88 B. B. Pan, J. Fan, J. Zhang, Y. Q. Luo, C. Shen, C. Q. Wang, Y. H. Wang and Y. G. Li, *ACS Energy Lett.*, 2022, **7**, 4224–4231.
89 J. Li, X. Li, C. M. Gunathunge and M. M. Waegele, *Proc. Natl. Acad. Sci. U. S. A.*, 2019, **116**, 9220–9229.
90 S. Weng, W. L. Toh and Y. Surendranath, *J. Am. Chem. Soc.*, 2023, **145**, 16787–16795.
91 M. Fan, J. E. Huang, R. K. Miao, Y. Mao, P. Ou, F. Li, X. Li, Y. Cao, Z. Zhang, J. Zhang, Y. Yan, A. Ozden, W. Ni, Y. Wang, Y. Zhao, Z. Chen, B. Khatir, C. P. O'Brien, Y. Xu, Y. C. Xiao, G. I. N. Waterhouse, K. Golovin, Z. Wang, E. H. Sargent and D. Sinton, *Nat. Catal.*, 2023, **6**, 763–772.
92 M. Esmaeilirad, Z. Jiang, A. M. Harzandi, A. Kondori, M. Tamadoni Saray, C. U. Segre, R. Shahbazian-Yassar, A. M. Rappe and M. Asadi, *Nat. Energy*, 2023, **8**, 891–900.
93 J. Timoshenko, A. Bergmann, C. Rettenmaier, A. Herzog, R. M. Aran-Ais, H. S. Jeon, F. T. Haase, U. Hejral, P. Grosse, S. Kuhl, E. M. Davis, J. Tian, O. Magnussen and B. Roldan Cuenya, *Nat. Catal.*, 2022, **5**, 259–267.
94 K. Ye, G. Zhang, B. Ni, L. Guo, C. Deng, X. Zhuang, C. Zhao, W.-B. Cai and K. Jiang, *eScience*, 2023, **3**, 100143.
95 R. V. Mom, L.-E. Sandoval-Diaz, D. F. Gao, C.-H. Chuang, E. A. Carbonio, T. E. Jones, R. Arison, D. Ivanov, M. Hävecker, B. Roldan Cuenya, R. Schlögl, T. Lunkenbein, A. Knop-Gericke and J.-J. Velasco-Vélez, *ACS Appl. Mater. Interfaces*, 2023, **15**, 30052–30059.
96 A. Bohme, J. C. Bui, A. Q. Fenwick, R. Bhide, C. N. Feltenberger, A. J. Welch, A. J. King, A. T. Bell, A. Z. Weber, S. Ardo and H. A. Atwater, *Energy Environ. Sci.*, 2023, **16**, 1783–1795.
97 X. Y. Wang, C. Y. Guo, B. W. Zhu, D. Z. Xiao, D. F. Gao, Z. Liu and F. Yang, *J. Chem. Phys.*, 2023, **158**, 204701.
98 L. C. Weng, A. T. Bell and A. Z. Weber, *Energy Environ. Sci.*, 2020, **13**, 3592–3606.
99 E. F. Johnson, E. Boutin, S. Liu and S. Haussener, *EES Catal.*, 2023, **1**, 704–719.
100 H. Mistry, F. Behafarid, R. Reske, A. S. Varela, P. Strasser and B. Roldan Cuenya, *ACS Catal.*, 2016, **6**, 1075–1080.
101 H. Simonson, W. E. Klein, D. Henckel, S. Verma, K. C. Neyerlin and W. A. Smith, *ACS Energy Lett.*, 2023, **8**, 3811–3819.
102 X. Wang, Q. Chen, Y. Zhou, Y. Tan, Y. Wang, H. Li, Y. Chen, M. Sayed, R. A. Geioushy, N. K. Allam, J. Fu, Y. Sun and M. Liu, *Nano Res.*, 2023, DOI: **10.1007/s12274-023-5910-9**.